ACS APPLIED MATERIALS & INTERFACES

Research Article

www.acsami.org

Magnetic Hyperthermia Ablation of Tumors Using Injectable Fe_3O_4/Calcium Phosphate Cement

Chunyan Xu,[†] Yuanyi Zheng,*[,†] Wei Gao,[†] Jinshun Xu,[†] Guoqing Zuo,[†] Yu Chen,[‡] Minzhu Zhao,[§] Jianbo Li,[§] Jinlin Song,[∥] Nan Zhang,[†] Zhigang Wang,[†] Hongyun Zhao,[†] and Zhechuan Mei*[,†]

[†]Chongqing Key Laboratory of Ultrasound Molecular Imaging, Second Affiliated Hospital of Chongqing Medical University, Chongqing, 400010 PR China

[‡]State Key Laboratory of High-Performance Ceramics and Superfine Microstructures, Shanghai Institute of Ceramics, Chinese Academy of Sciences, 1295 Ding-Xi Road, Shanghai 200050, PR China

[§]Department of Forensic Medicine, Chongqing Medical University, Chongqing, 400000 PR China

[∥]Affiliated Stomatological Hospital of Chongqing Medical University,Chongqing, 400000 PR China

Supporting Information

ABSTRACT: In this work, we have developed an injectable and biodegradable material using CPC containing Fe_3O_4 nanoparticles for minimally invasive and efficiently magnetic hyperthermia ablation of tumors. When exposed to an alternating magnetic field, the MCPC could quickly generate heat. The temperature of PBS and the excised bovine liver increased with the MCPC weight, iron content, and time. The ablated liver tissue volume for 0.36 g of 10% MCPC was 0.2 ± 0.03, 1.01 ± 0.07, and 1.96 ± 0.19 cm^3, respectively, at the time point of 60, 180, and 300 s. In our in vivo experiment, the MCPC could be directly injected into the center of the tumors under the guidance of ultrasound imaging. The formed MCPC was well-restricted within the tumor tissues without leakage, and the tumors were completely ablated by 0.36 g of 10% injectable MCPC after 180 s of induction heating.

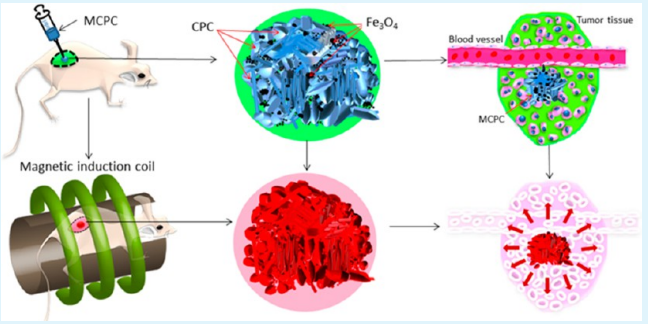

KEYWORDS: *magnetic hyperthermia ablation, injectable, biodegradable, calcium phosphate cement, tumor*

INTRODUCTION

For most cancer patients, the first choice for treatment is still surgery, although its physical and psychosocial impacts on patients (such as large trauma, surgery-related complications,[1] and the cosmetic outcome, especially for women)[2] have aroused wide concern. Thus, minimally invasive treatment has become increasingly attractive in recent years.[3−5] Radiofrequency ablation, laser-induced thermal therapy, microwave ablation, cryoablation, and focused ultrasound are currently the most widely used minimally invasive procedures.[4] However, these strategies have their limitations, such as tumor reoccurrence, skin burns, ecchymosis, and skin puckering, which restrict their extensive clinical applications.[3]

As a potential minimally invasive choice, magnetic induction hyperthermia has been extensively studied by Gilchrist et al. since 1957.[6,7] Gilchrist proposed the hypothesis that tumors might be treated using heat generated by a magnetic substance upon exposure to an alternating magnetic field, which was taken as an efficient strategy without systemic toxicity.[8] The currently used magnetic media for magnetic induction hyperthermia includes implanted ferromagnetic thermoseeds,[9] intravenous magnetic nanoparticles, and magnetic fluid.[10] The thermoseeds require precise and relatively complex calculation and control,[11] and the removal of magnetic thermoseeds needs an additional surgical operation due to the lack of degradation in the body. For the nanoparticles or magnetic fluid, it is difficult to accumulate a sufficient amount of magnetic nanoparticles to the target tissue,[12] and it is easy for them to leak into the surrounding tissue or blood vessels, which not only lowers the ablation efficiency but also is a hidden concern for safety. Yu Chen et al. reported poly(lactic-*co*-glycolic-acid) carrying iron powder (S−Fe/PLGA) for the magnetic hyperthermia ablation of tumors,[13] while the organic solvent *N*-methylpyrrolidone (NMP) was used in the preparation of S−Fe/PLGA and would be injected into the tissue. NMP is on the list of chemicals known to cause cancer or reproductive toxicity as cited in California Proposition 65 (1986).[14,15] Moreover, S−Fe/PLGA at a low PLGA/NMP ratio will leak into the blood, resulting in thrombus in the vasculature, which causes potential safety concerns.

Thus, to develop an injectable magnetic media with a better capability of confining the iron particles inside the targeting

Received: March 13, 2015
Accepted: June 12, 2015
Published: June 12, 2015

DOI: 10.1021/acsami.5b02077
ACS Appl. Mater. Interfaces 2015, 7, 13866−13875

tissue to avoid the leakage into blood or surrounding tissues and without using organic solvent or any other toxic materials, it is of importance for the bench-to-bed translation of the magnetic hyperthermia ablation technique. Since its first report in the 1980s by Brown et al, calcium phosphate cement (CPC) has attracted great attention worldwide because of its excellent self-setting ability, biocompatibility, and biodegradation. Moreover, CPC has a low setting temperature, and the phase-transformation ability to form a solid material in situ[16,17] Among the many liquid phases for the calcium phosphate cement, polyethylene glycol 600 (PEG-600) has a good safety record and is widely used in drug production to increase the dispersibility, dissolvability, and biocompatibility of nanomaterial.[18,19]

Inspired by the phase-transformation behavior of CPC, we therefore consider distributing Fe_3O_4 nanoparticles inside the calcium phosphate cement with PEG-600 as the liquid phase, expecting to develop a highly efficient, injectable, and phase-transitional magnetic material for minimally invasive magnetic ablation of the tumor. This material was expected to form a solid in situ that can confine the Fe_3O_4 nanoparticles inside the tissue, avoiding the leaking into surrounding tissues to further improve the safety as well as improving the efficiency for induction heating. By applying an alternating magnetic field, we expect that magnetic calcium phosphate cement (MCPC) will quickly and efficiently generate heat and raise the temperature inside the tumor for tumor ablation therapy. The MCPC is biodegradable, which can avoid the adverse effects associated with the long-term retention of foreign materials in tissue. Moreover, the MCPC set in situ can also be repeatedly used to generate heat for the ablation of tumor residue or local recurrence without performing another interventional procedure if the tumor residue or local recurrence was found before the complete degradation of MCPC.

MATERIALS AND METHODS

Preparation of Magnetic Calcium Phosphate Cement. The β-tricalcium phosphate (β-TCP, $Ca_3(PO4)_2$, 55% mass fraction, Ensall Beijing Co., Ltd.) and monocalcium phosphate monohydrate (MCPM, $Ca(H_2PO_4)_2{\cdot}H_2O$, 45% mass fraction, Tianjin DaMao Chemical Reagent Factory) were premixed at a molar ratio of 1:1 to obtain the calcium phosphate cement powder base (CPC).[20] The magnetic calcium phosphate cement (MCPC) was prepared by adding the Fe_3O_4 magnetic nanoparticles (Chengdu AikeDa Chemical Reagent Co., Ltd.) into the CPC at an iron/CPC weight ratio of 0, 5, 10, and 15% and mixed with polyethylene glycol 600 (PEG 600, Wuhan Boster Biological Technology Co., Ltd.) at the liquid−solid ratio (L/S) of 0.5.

Volume−Mass Conversion. The MCPC paste was loaded into a syringe, and then 0.1, 0.2, and 0.3 mL of MCPC were injected. The weight of the MCPC was measured after drying. All of the following MCPC weights were calculated based on results of the volume−mass conversion study.

Morphology Characterization of MCPC. The morphology of the MCPC (iron content: 10%) was determined by scanning electron microscope (SEM, AMETEK EDAX, S-3700, 371027−02, America) at an accelerating voltage of 5 kV and a working distance of 7.1 mm. Elemental analysis was performed using an energy dispersive X-ray spectrometer (EDS, AMETEK, EDAX, S-3700, 371027−02, NJ, U.S.A.) at an accelerating voltage of 15 kV and a working distance of 10 mm. The magnification for SEM image was 10 000×, and for EDS, images were 5000×. To improve the surface conductivity, we dried the sample for 24 h and placed it on carbon conductive tape.[21]

Washout Resistance Ability Test. The washout resistance was tested using a method reported by Han, et al.[20] In short, the MCPC paste (iron content: 5, 10, and 15%) was manually shaped into an 8 mm diameter ball and then immediately placed into the phosphate-buffered solution (PBS, pH 7.4) in a glass culture dish on a heating device. The material was considered to pass the washout resistance test if the MCPC ball did not visibly disintegrate in aqueous solution until the temperature increased to 150 °C. The washout resistance of the MCPC paste was evaluated visibly by the extent of the disintegration.

Injectability. The injectability of MCPC was evaluated by the "injectable percentage" using a method reported by Burguera EF.[22] In short, the compression started at the time point of 1.5 min after the start of mixing, and the cement was extruded at a crosshead speed of 15 mm/min. The injection continued until either all of the paste was extruded or a maximum force of 300 N was reached.

$$\text{injectable percentage}\ (\%) = V_{\text{inj}}/V_{\text{total}}$$

where V_{inj} is the volume of injected MCPC from the syringe (volume, 10 mL; the inner diameter of the needle, 1.6 mm) and V_{total} is the total volume of MCPC in the syringe before injection.

Degradability. The degradability was measured using a method reported by Han, et al.[20] In short, the 0.5 g of MCPCs (iron content: 0, 5, and 10%) was prepared and put in 4 mL of 37 °C PBS stirred by a magnetic rotor to generate circulating flow to mimic the blood flow in vivo. The weights of the MCPCs were measured on the 1st, 3rd, 5th, 8th, 11st, 18th, 25th, 32nd, 38th, and 68th day. The percentage of weight loss was used to evaluate the degradability using the following formula:

$$\text{degradability}\ (\%) = (W_{\text{i}} - W_{\text{deg}})/W_{\text{i}}$$

where W_{i} is the initial weight of MCPC and W_{deg} is the weight after degradation.

Exotherm during the Setting Reaction. The exotherm during the setting reaction was measured using a method reported by Kawashita et al.[23] The 5 g of 0, 5, and 10% MCPCs were manually shaped into a ball within 3 min, and a mercury thermometer was inserted to continuously measure the temperature change during the setting reaction. The increased temperature between the room temperature and the peak temperature of the thermometer was taken as the exotherm during the setting reaction.

Evaluation of Induction Heating Efficiency in PBS. The MCPCs with different weights and with different iron contents (0.19 g of 10%, 0.36 g of 10%, 0.54 g of 10%,0.54 g of 5%, 0.54g of 0%, and 0.54 g of 10% MCPCs after degradation) were placed in 1 mL of PBS in a cylindrical hole (0.7 cm × 0.7 cm) of an agarose gel (2 cm × 2 cm × 2 cm). The MCPCs were exposed to an alternating magnetic field by a homemade magnetic hyperthermia analyzer (frequency 626 kHz, output Current 28.6 A, coil diameter 3 cm)[13] for 300 s, and the peak surface temperature of PBS was continuously acquired by a far-infrared thermometer (Fluke Ti32, Fluke Corporation, U.S.A.). The thermal images were analyzed via the SmartView 3.6 software.

Evaluation of Heating Efficiency in Excised Bovine Liver. On the basis of the above experiments, 10% MCPC was selected for further study. The 10% MCPCs with different weights (0.19, 0.36, and 0.54 g of 10%) were implanted into the freshly excised bovine liver parts (6 cm × 2 cm × 2 cm) and exposed to the same alternating magnetic field for 300 s. The peak surface temperature of liver was continuously acquired by a far-infrared thermometer (Fluke Ti32, Fluke Corporation, U.S.A.), and the temperature at different distances (0, 1, 2, and 3 cm) to the peak surface temperature was recorded at the time point of 300s.

Evaluation of Ablation Efficiency in Excised Bovine Liver. The 0.19, 0.36, and 0.54 g of 10% MCPCs were implanted into the freshly excised bovine liver (2 cm × 2 cm × 2 cm) and exposed to the same alternating magnetic field as above for 60, 180, and 300 s. The ultrasound echo intensities were monitored by ultrasound imaging. The ablated tissue volumes were calculated using the following formula:[24]

$$V_{\text{a}} = D_{\text{l}}D_{\text{s}}^2/2$$

DOI: 10.1021/acsami.5b02077
ACS Appl. Mater. Interfaces 2015, 7, 13866−13875

Table 1. Volume−Mass Conversion

	0.1 mL	0.2 mL	0.3 mL
weight after drying (g)	0.19 (0.192 ± 0.008)	0.36 (0.359 ± 0.010)	0.54 (0.539 ± 0.009)

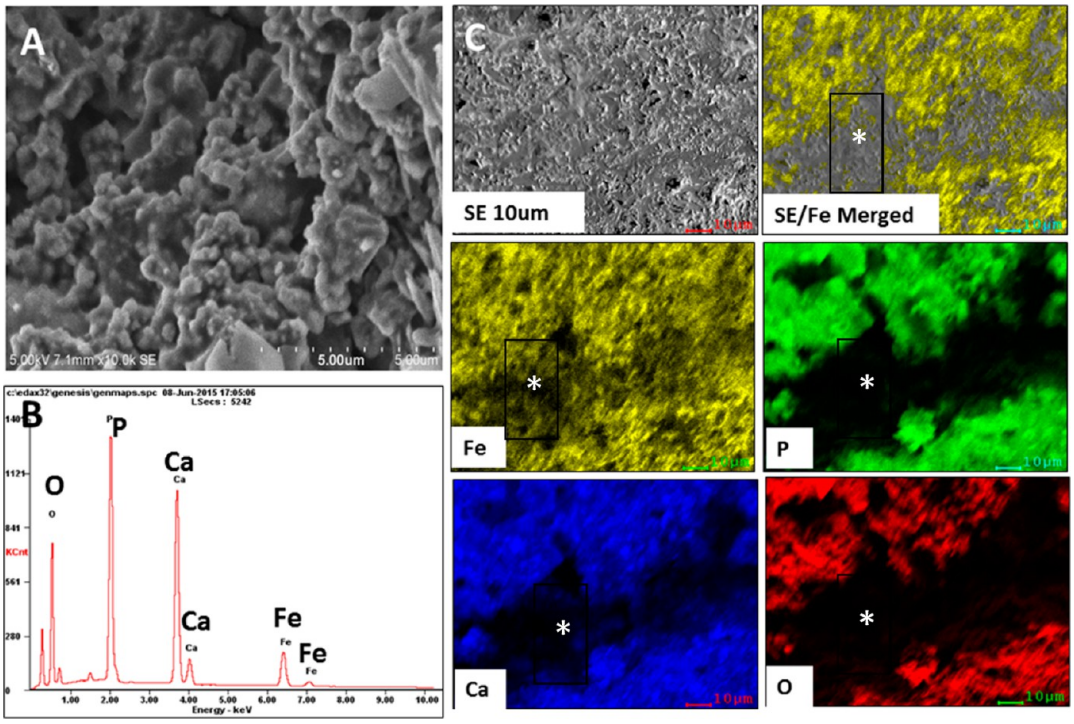

Figure 1. SEM and EDS map scan images for 10% MCPC. (A) The SEM image showed that the MCPC matrix was porous. (B) Element energy spectrum by EDS map scan. (C) The EDS map scan images showed that the Fe element was well-distributed within the matrix of CPC. The darker area reflected the rough surface of the MCPC matrix.

where V_a is the ablation volume (cm^3), D_l is the long diameter of the ablated tissue measured by ruler, and D_s is the short diameter of the ablated tissue measured by ruler.

Preparation of Nude Mouse MB231 Human Breast Cancer Xenograft. The human breast cancer xenografts were built on 12 female SPF nude mice (4 weeks old) with a mean body weight of 15 g according to a method in the literature.[25] The MB231 cancer cells were collected by centrifugation and dispersed into axenic PBS, followed by a subcutaneous injection of 1×10^5 cells per tumor into the backs of 12 female SPF nude mice. The mice were used for experiments when the tumor volume reached 1.90 ± 0.67 cm^3. All the animal procedures were conducted under the guidelines approved by the Chongqing Medical University.

The tumor volumes were calculated using the following formula:

$$V_t = D_l D_s^2/2$$

where V_t is the tumor volume (cm^3), D_l is the long diameter of the tumor measured by ruler, and D_s is the short diameter of the tumor measured by ruler.

Evaluation of Magnetic Thermal Ablation Efficiency in Vivo. The 12 nude mice were divided into two groups and were anesthetized by pentobarbital (0.08−0.1 mL/mouse, 1%). For group 1, eight mice were randomly selected, and 0.2 mL (0.36 g) of 10% injectable MCPCs were injected into the tumors under the real time guidance of ultrasound imaging (Esoate, L5−12 MHz). The ultrasound images were recorded, and the echo intensities of MCPCs were measured. Then, the mice were exposed to the alternating magnetic field as above for 180 s, the surface temperature of the tumors were continuously acquired by the same infrared thermometer as above, and the temperature at different distances (0, 0.5, 1, 2, and 3 cm) to the core surface temperature was recorded at the time point of 180 s. Immediately after the ablation treatment, three mice were randomly selected and euthanized for tumor pathology examination by hexatoxylin and eosin (H & E) staining. The other five mice were fed for further observation of the tumor growth trend. For group 2, the other four mice without any treatment were taken as the control group.

Statistical Analysis. All statistical analysis were performed using the Statistical Package for the Social Sciences 18.0 (SPSS, Inc., Chicago, IL), and p value <0.05 was considered statistically significant. All results are presented as mean ± STDEV (standard deviation). For multiple comparisons, ANOVA (differences in tumor volumes, injectable percentage, temperature, and echo intensity) was used when the data were normally distributed and with homogeneous variance, and rank sum tests were used in other cases. Once significant differences were detected, Student's t-tests were used for comparisons between two groups.

RESULTS

Volume-to-Mass Calculation. The volume−mass conversion results showed that the masses after drying were 0.192 ± 0.008, 0.359 ± 0.010, and 0.539 ± 0.009 g for 0.1, 0.2, and 0.3 mL of MCPC separately (Table 1).

Morphology. The SEM image (Figure 1A) showed that the MCPC matrix was porous. The EDS map scan image (Figure 1C) showed that the Fe element was well-distributed within the matrix of CPC. The corresponding element energy percentages spectrum was shown in Figure 1B. The energy percentages for Ca, P, O, and Fe were 21.2, 18.9, 49.85, and 10.05%, respectively.

Antiwashout. The 5 and 10% MCPC were resistant to washout and were kept integrated without any disintegration

DOI: 10.1021/acsami.5b02077
ACS Appl. Mater. Interfaces 2015, 7, 13866−13875

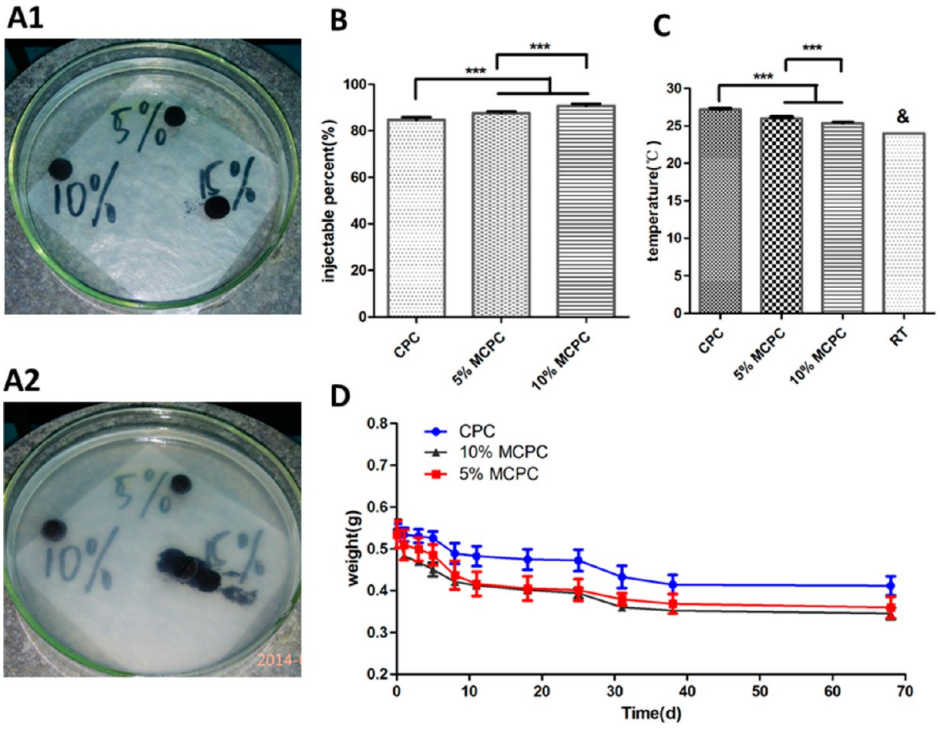

Figure 2. (A) The antiwashout experiment (A1: preheating, A2: postheating). (B) Injectability of MCPC (***: significant difference ($p < 0.05$)). (C) The exotherm during the setting reaction for MCPC (RT, room temperature; ***, significant difference ($p < 0.05$) for different concentrations of Fe_3O_4 nanoparticles; &, significant difference ($p < 0.05$) CPC vs RT). (D) The time−weight loss curve of MCPC after 1, 3, 5, 8, 11, 18, 25, 32, 38, and 68 days.

even the temperature reached 150 °C in the washout resistance test (Figure 2A1, before heating; Figure 2A2, after heating), while the 15% MCPC disintegrated into numerous small fragments when the temperature reached 50 °C.

Injectability. As shown in Figure 2B, the injectable percentage was 84.68 ± 1.13, 87.5 ± 0.75, and 90.68 ± 0.92% for 0, 5, and 10% MCPC, respectively. The statistical analysis show that 0% MCPC versus 5% MCPC and 10% MCPC have significant differences ($p < 0.05$), and 5% MCPC versus 10% MCPC also has a significant difference ($p < 0.05$) in the injectable percentage, which showed that the injectability increased with the iron content.

Exotherm during the Setting Reaction. As shown in Figure 2C, the exotherm during the setting reaction for MCPC was low. Under room temperature (RT), the exotherms during the setting reaction were 3.17 ± 0.18, 1.99 ± 0.17, and 1.36 ± 0.14 °C for CPC, 5% MCPC, and 10% MCPC, respectively. The statistical analysis show that CPC versus RT have significant differences ($p < 0.05$), and CPC versus 5% MCPC and 10% MCPC have significant difference ($p < 0.05$). Furthermore, 5% MCPC versus 10% MCPC also has a significant difference ($p < 0.05$) in the exotherm during the setting reaction, which means that the Fe_3O_4 nanoparticles may reduce the exotherm in the setting reaction.

Degradability. The time−weight loss curve of MCPC (Figure 2D) showed that the MCPC was degradable with time. In Figure 2D, the percentages of weight loss were 24.23 ± 0.02, 32.62 ± 0.03, and 37.38 ± 0.03% for 0.5 g of CPC, 5% MCPC, and 10% MCPC, respectively, after soaking in PBS for 68 days.

Heating Efficiency in PBS in Vitro. When exposed to the alternating magnetic field, the color of the thermal images (Figure 3A) showed the 10% MCPC could quickly generate a lot of heat to increase the temperature of PBS, and this temperature increased with the MCPC weight, iron content, and time. The corresponding time−temperature curve confirmed this finding (Figure 3B). The temperature reached to 85.17 ± 4.95, 97.83 ± 5.78, and 125.63 ± 28.17 °C, respectively, for the 0.54 g of 10% MCPC at the time point of 60, 180, and 300 s ($p < 0.05$), but the temperature only reached 35.00 ± 0.10 and 84.13 ± 4.28 °C for the 0.54 g of 0% and 5% MCPC, respectively, after 300 s of magnetic induction heating ($p < 0.05$). For 0.19 and 0.36 g of 10% MCPC, the temperature reached 80.83 ± 10.49 and 91.73 ± 4.1 °C, respectively, after 300 s of induction heating ($p < 0.05$). Even after 68 days of degradation, the 0.54 g of 10% MCPC still maintained a good heating efficiency (Figure 3C).

Heating Efficiency in Excised Bovine Liver. The thermal images acquired from the surface of the 6 cm × 2 cm × 2 cm excised bovine liver containing 0.19, 0.36, and 0.54 g of 10% MCPC showed the surface temperature increased with the time and the weight of MCPC (Figure 4A). The corresponding temperature curve confirmed this finding (Figure 4B). The peak surface temperature of the excised bovine liver containing 0.54 g of 10% MCPC reached 27.67 ± 0.61, 45.37 ± 3.59, and 68.7 ± 9.20 °C, respectively, at the time point of 60, 180, and 300 s ($p < 0.05$), and the temperature at different distances to the location of the MCPC decreased significantly with distance ($p < 0.05$). We also found the peak surface temperature of the liver increased with the weight of the MCPC. The peak surface temperature containing 10% MCPC reached 34.20 ± 3.95 and 46.57 ± 3.29 °C, respectively, for 0.19 and 0.36 g of MCPC after 300 s of induction heating ($p < 0.05$) (Figure 4B).

Ablation Efficiency in the Excised Bovine Liver. The excised bovine liver parts containing the 10% MCPCs were visible under ultrasound imaging. The ultrasound echo intensity had a tendency to increase with the weight of the MCPCs and

DOI: 10.1021/acsami.5b02077
ACS Appl. Mater. Interfaces 2015, 7, 13866−13875

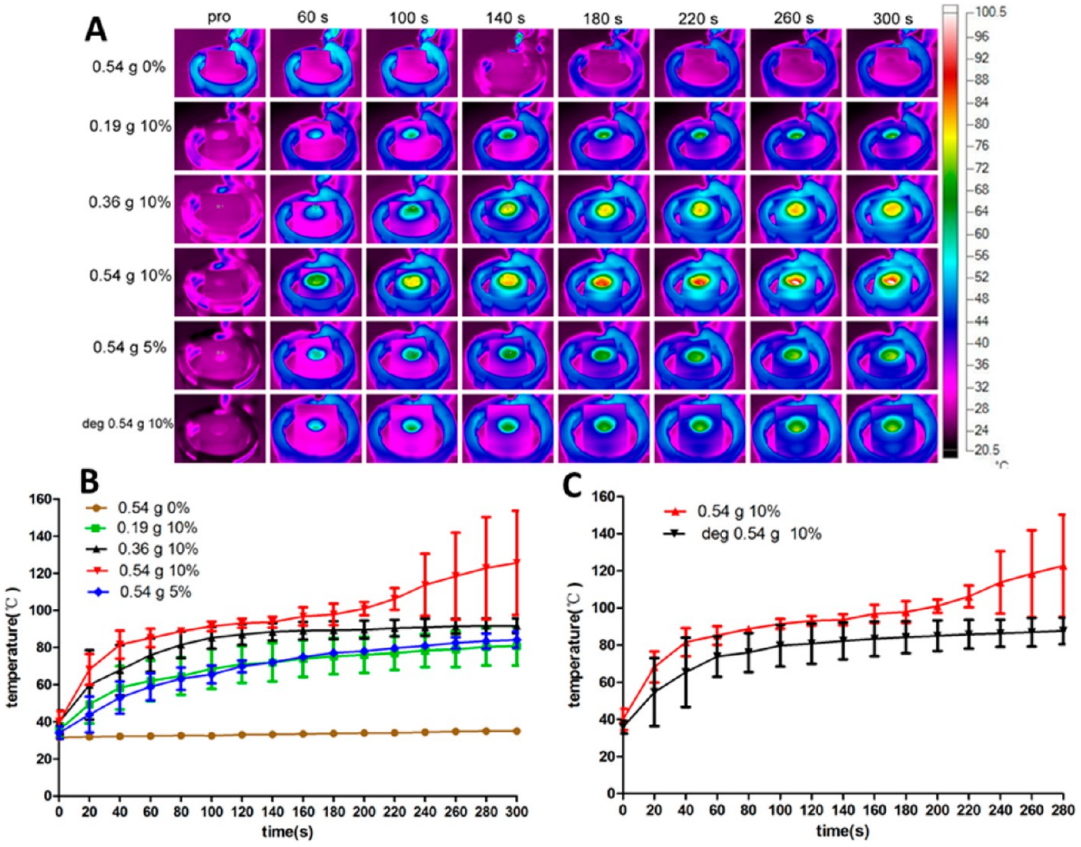

Figure 3. Heating efficiency of the MCPC. (A) The thermal images for different weights and iron contents of MCPC at different magnetic induction times. (The "deg 0.54 g 10%" in parts A and C of Figure 3 represents 0.54 g of 10% MCPC after degradation for 68 days.) (B) The corresponding time−temperature curve of the MCPCs with different weight and iron content. (C) The corresponding time−temperature curve for 0.54 g of 10% MCPC after 68 days of degradation.

the extended time under the alternating magnetic field, and it was difficult to give a quantitative analysis because of the effects of the ultrasound shadowing behind the MCPCs (Figure 5A). After 60, 180, and 360 s of magnetic induction heating, the ablated liver tissue around the MCPC showed a pale color when observed with the naked eye when each of the bovine liver part was split into two parts for observation (Figure 5B). The ablated area increased with the weight of the MCPC and the extended time under alternating magnetic field. The ablated tissue volumes for the 0.36 g 10% MCPC were 0.2 ± 0.03, 1.01 ± 0.07, and 1.96 ± 0.19 cm^3, respectively, at the time point of 60, 180, and 360 s ($p < 0.05$) (Figure 5C).

Magnetic Hyperthermia Ablation Efficiency in Tumor Xenograft. As Figure 6A showed, the tumors were elliptical in shape and appeared hypoechoic in ultrasound imaging. The needle was clearly visible under real time ultrasound imaging, which ensured precision in the in situ injection of the MCPC. The MCPC was hyperechoic, with an acoustic shadow after the injection. The ultrasound images showed a good distribution of the MCPC inside the tumor, with a wirelike shape on the longitudinal section and a spotlike shape on the transverse section. The thermal images (Figure 6B) and the corresponding time−temperature curve (Figure 6C) obtained from the tumor area confirmed the heating efficiency of 0.36 g of 10% MCPC. The peak surface temperature of the tumor containing the MCPC could reach to 74.73 ± 9.12 °C after magnetic induction heating for 180 s. Figure 6 D shows that the temperature at different distances to the core temperature decreased significantly with distance after 180 s of magnetic induction heating ($p < 0.05$).

As shown in Figure 7A, the significantly macroscopic changes of the tumors were observed after the magnetic ablation. The color of the skin on top of the tumors turned into a pale white color immediately after the magnetic hyperthermia ablation treatment. On the first day after the ablation treatment, the color of the tumors including the above skin turning into black, with a clear boundary between the ablated and nonablated tissue. During the next 2 days, the tumor tissue (including the skin above) began to form a scab. On the fourth day, the crust of the black necrotic tissue began to desquamate. After 1 week, the size of the tumors was obviously diminishing. After 2 weeks, the black necrotic tissue began to separate from the body and fell off. The microscopic therapeutic outcomes of tumor cells were evaluated by the typical H & E staining. Large areas of disorder tissue with remarkably destructed cells and uniformly red-stained cytoplasm were found in the tumor tissue that received MCPC followed by magnetic ablation. Comparatively, the control mouse showed no obvious cell destruction, and had an integrated nucleus and cytoplasm (Figure 7B). The time−tumor volume curve revealed the manifested reduction tendency in the tumor volume after magnetic ablation, while the tumor volume in the control group continued to increase (Figure 7C).

DISCUSSION

In this study, we have developed an injectable and phase-transitional magnetic material by distributing Fe_3O_4 nano-

DOI: 10.1021/acsami.5b02077
ACS Appl. Mater. Interfaces 2015, 7, 13866−13875

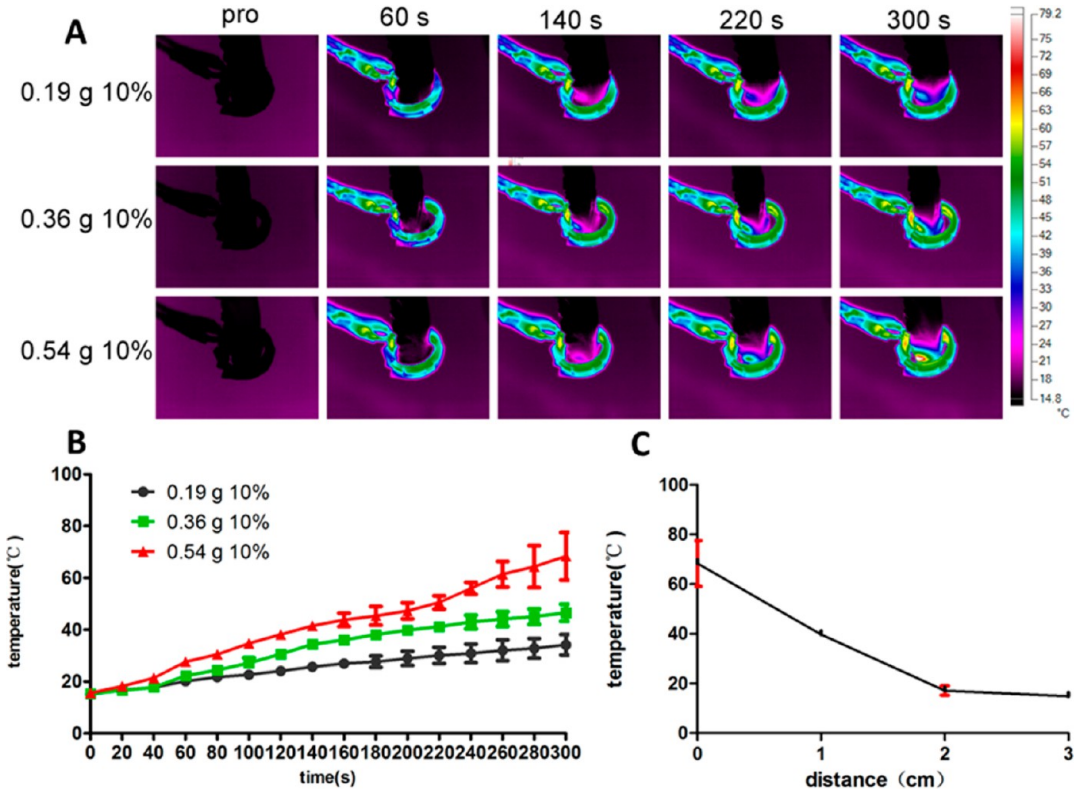

Figure 4. Heating efficiency in the 6 cm × 2 cm × 2 cm excised bovine liver. (A) Thermal images of the excised bovine liver containing 0.19, 0.36, and 0.54 g of 10% MCPC when exposed to the alternating magnetic field for 300 s. (B) The corresponding time−temperature curve. (C) The distance−temperature curve for 0.54 g of 10% MCPC embedded in the excised bovine liver after 300 s of induction heating.

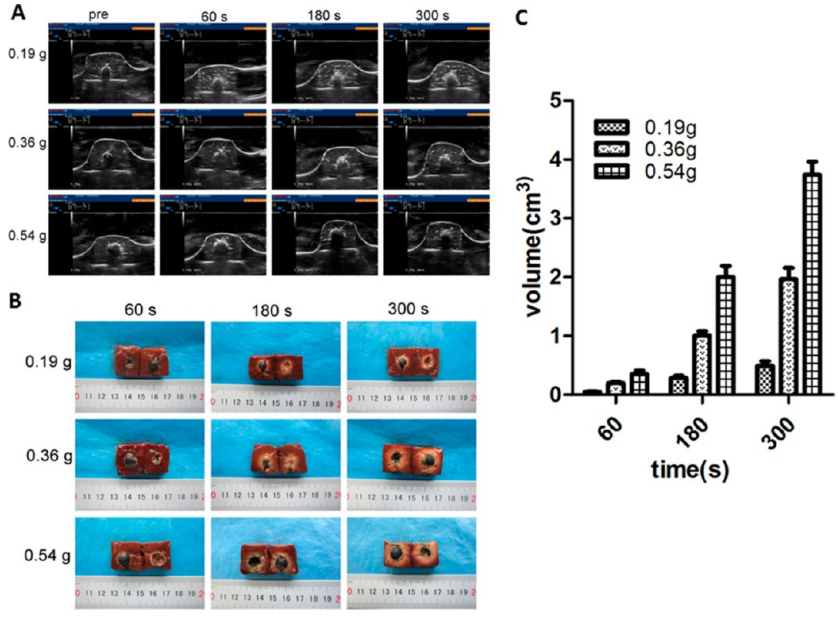

Figure 5. Ablation efficiency correlated to the MCPC weight and the extended time under the alternating magnetic field. (A) The ultrasound imaging of the excised bovine liver containing 0.19, 0.36, and 0.54 g of 10% MCPC at the time point of 60, 180, and 300 s after ablation. (B) The corresponding macroscopic photos. (C) The corresponding necrosis volume.

particles inside the calcium phosphate cement for the minimally invasive magnetic ablation of tumors. We used PEG-600 with a good safety record as the liquid phase to prepare the MCPC without using organic solvent. The injection of this biodegradable MCPC was guided and monitored by real-time ultrasound, and the MCPC was visible to CT imaging as well, which should add value to its safety use in future clinical application. Furthermore, the MCPC showed a high-efficiency property in the magnetic hyperthermia ablation of tumor.

The CPC is a hydroxyapatite compound with a structure similar to that of human bone, which has been extensively applied in the field of clinical orthopedics, such as

DOI: 10.1021/acsami.5b02077
ACS Appl. Mater. Interfaces 2015, 7, 13866−13875

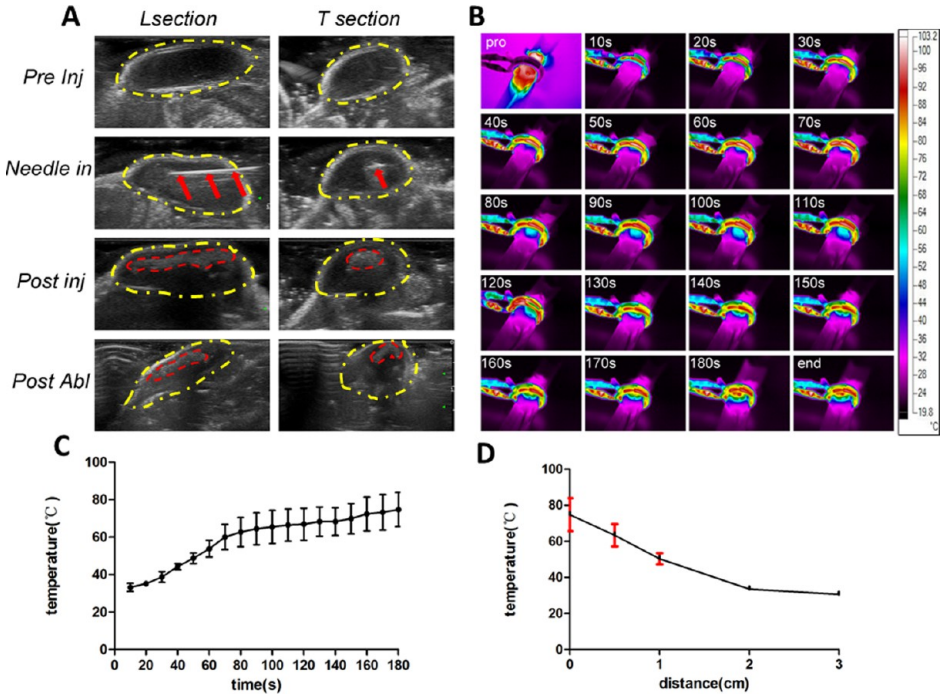

Figure 6. Ultrasound-guided injection and the tumor surface temperature monitoring. (A) Ultrasound-guided injection and the ultrasound imaging of the injected 0.36 g of 10% MCPC in tumor pre- and post-180 s of magnetic induction heating. (L section: longitudinal section. T section: transverse section. Pre Inj: pre-injection. Post inj: post-injection. Post abl: post-ablation. Yellow dotted line: tumor. Red dotted line: MCPC. Red arrows: needle). (B) The thermal images of tumor containing 0.36 g of 10% MCPC that was exposed to an alternating magnetic field for 180 s. (C) The corresponding time−temperature curve. (D) The distance−temperature curve for 0.36 g of 10% MCPC embedded in the tumor after 180 s of magnetic induction heating.

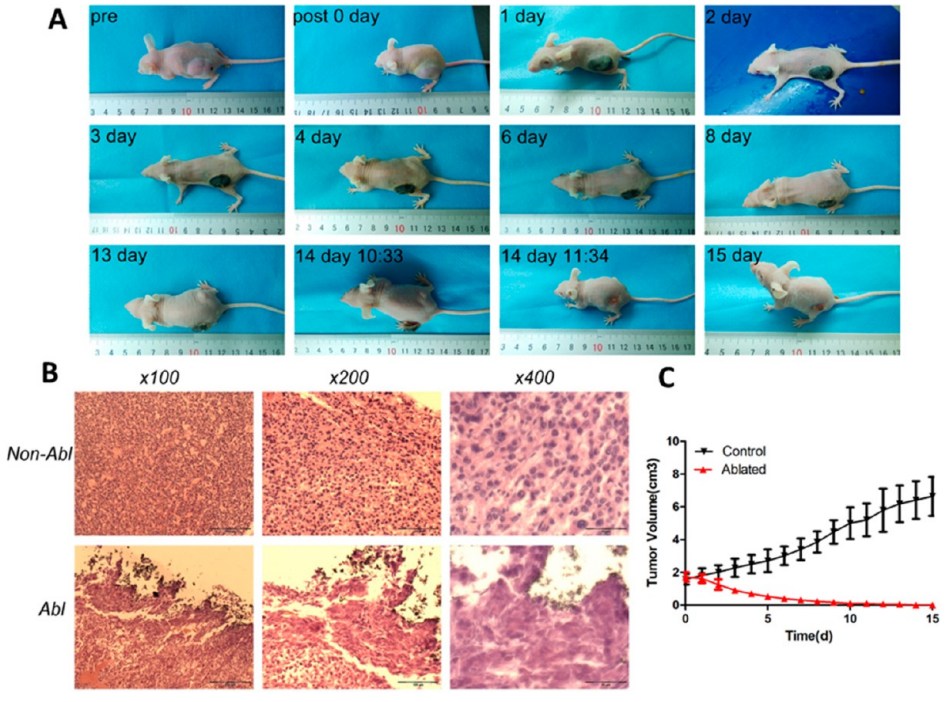

Figure 7. Magnetic hyperthermia ablation efficiency in tumor model. (A) The macroscopic changes of tumor during the 2 weeks after the magnetic hyperthermia ablation treatment. (B) The microscopic structure of the ablated and nonablated tumor tissue. (C) The time−tumor volume curve.

osteoporosis,[26] bone tumors with pathologic fractures,[27] and chronic osteomyelitis.[28] In this study, the microstructure of the MCPC was porous, and the Fe_3O_4 nanoparticles were uniformly distributed within the CPC. The amount of Fe_3O_4 nanoparticles inside the CPC should be controlled because the 15% MCPC did not behave well in the antiwashout test, which means that the Fe_3O_4 nanoparticles could "escape" from the MCPC once the amount of Fe_3O_4 nanoparticles reached a certain threshold (for example, 15%). The 5% and 10% MCPCs were resistant to washout and stayed integrated even when the

DOI: 10.1021/acsami.5b02077
ACS Appl. Mater. Interfaces 2015, 7, 13866−13875

temperature increased to 150 °C, which means they might prevent the Fe_3O_4 magnetic nanoparticles from permeating into the surrounding tissues or blood vessels in vivo, and they could be kept integrated during the magnetic induction hyperthermia treatment.

The injectability study showed the injectable percentage of the 10% MCPC was 90.68 ± 0.92%, which guaranteed the local injection of the MCPC in a minimally invasive manner. The exotherm during the setting reaction was considerably low for the 10% MCPC, which was 1.36 ± 0.14 °C and should be much safer than PMMA, which has a much higher exotherm of 95 °C in polymerization.[29] The degradability test showed that the MCPC was degraded with time. The in vitro magnetic heating efficiency study showed that the MCPC could quickly heat the PBS and the excised bovine liver under an alternating magnetic field, and the ablation efficiency increased with the time, the MCPC weight, and the iron content, which means the ablation volume is controllable. We found that even when the heating efficiency of the MCPC gradually decreased after a period of time, it still could increase the local temperature to the specific level needed for the ablation of tumors. Thus, the MCPC might be able to be used repeatedly for the ablation of the locally recurrent tumor without the need for the reinjection of the MCPC. Further in vivo study showed the injectable and biocompatible MCPC could efficiently generate enough heat to completely ablate the tumor model. However, a shorter time is needed to ablate tumor tissue than for the same volume of the excised bovine liver tissue. The reason might owe to the heterogeneity between tumor tissue and excised bovine liver tissue, which leads to a nonuniform response to heat treatment. The tumor cells were reported to be more sensitive to heat than the normal cells; thus, the tumor tissue could be completely ablated in a shorter time and lower temperature.[29]

For the future clinical translation, the safety issue of MCPC has to be a concern, especially the degradability of the MCPC. Some research in the literature has shown that the CPC implant could be biodegraded in soft tissues. Bing Han et al.[20] reported the implantation of this brushite in the subcutaneous tissue in rabbits and found that 43% of the initial amount of the subcutaneously implanted brushite in rabbits had degraded in 12 weeks. Uwe Klammert et al.[30] reported the effects of a long-term intramuscular implantation regime on the dissolution of various low-temperature-setting calcium phosphate cements including brushite in vivo and found no indication for wound infections, inflammation, or rejection until the retrieval of the implants after 15 months; they found that the implanted volume showed a significant reduction, too. Ooms et al.[31] implanted the CPC in the back of goats and found small areas of calcification in the fibrous capsule surrounding the implants in 4 to 8 weeks. On the basis of this finding, they proposed that the CPC is biocompatible and can be used next to soft tissue. On the issue of the biodegradation mechanism of CPC, Uwe Klammert et al.[30] reported that the degradation was accompanied by both a distinct extent of cement dissolution as well as the changes of the phase composition of the retrieved cement implants. Jianxi Lu et al.[32] reported that biodegradation of the Ca−P biomaterials in tissue might be a combination of the following processes: (1) physical (abrasion, fracture, disintegration); (2) chemical (dissolution, increases of Ca and P locally at the surface); and (3) biological (reductions in pH caused by cellular and phagocytic activities resulting in increases in the rate of biodegradation due to the dissolution of the Ca−P biomaterials). However, the possibility of inducing calcification in soft tissue for MCPC is still a potential safety issue and needs to be further studied. The another main component of the MCPC is the Fe_3O_4 nanoparticles, which have a good biocompatibility and safety profile[33] and have been authorized for clinical application by the FDA as a magnetic resonance imaging contrast agent.[34] Another safety issue is the damage to the normal tissue, which is the same safety issue for the other hyperthermia techniques such as radiofrequency ablation or microwave ablation. Fortunately, in clinical applications, to avoid potential recurrence of tumor the normal tissue beyond the tumor was routinely ablated as well.[35] In this study, we found that sometimes, the normal skin tissue close to the subcutaneous tumor was damaged and peeled off with the necrotic tumor, while the muscle tissue close to the tumor was not significantly affected by the complete ablation of tumor. The detailed mechanism is unknown. We would like to investigate these mechanisms in our future study.

Finally, the safety issue of the leakage of MCPC into the surrounding tissue is of concern too. In our preliminary study, we compared the MCPC with pure Fe_3O_4 nanoparticles in the capability of leakage. We put the pure Fe_3O_4 nanoparticles and the MCPC into the holes of an agarose gel for magnetic induction heating. The results showed that the flow ability of the pure Fe_3O_4 nanoparticles was significantly increased with the temperature rise, and they flowed everywhere when the temperature reached 90−100 °C (file "SI-movie 1", Supporting Information). For the MCPC, however, the Fe_3O_4 nanoparticles were tightly confined in the CPC even when the temperature was increased to 124 °C (file "SI-movie 2", Supporting Information), and the MCPC stayed integrated during the whole magnetic induction heating process. Thus, we propose that it has a better safety record compared to that of the pure Fe_3O_4 nanoparticles, which have been well-employed in much research via direct tumor injection.

Although we have proved the feasibility of using the novel MCPC material for the treatment of tumors, there are still some limitations for this study. First, the surface temperature acquired by the thermal images could not accurately reflect the internal temperature. The recently developed MR thermometry has been shown as an encouraging prospect, and is considered to be a very useful method for the precise method for the intraprocedural evaluation of temperature.[36,37] Second, incomplete ablation might happen if the tumor is irregular and in deep tissue. In this study, the superficial xenograft tumor model with a good shape was used, and the injection of MCPC was guided by real-time ultrasound imaging to deliver the MCPC homogeneously inside the tumor along the long axis of the tumor so that the incomplete ablation of tumor was successfully avoided.

CONCLUSIONS

We have developed an injectable and biodegradable material using CPC containing Fe_3O_4 nanoparticles for the highly efficient and minimally invasive magnetic ablation of tumor. We expect that this developed magnetic hyperthermia ablation technique could contribute to the clinical application of minimally invasive techniques for the treatment of tumors and offer a better cosmetic outcome with fewer complications.

ASSOCIATED CONTENT

Supporting Information

Videos showing the magnetic induction heating of pure Fe_3O_4 nanoparticles and the MCPC in the holes of an agarose gel

DOI: 10.1021/acsami.5b02077
ACS Appl. Mater. Interfaces 2015, 7, 13866−13875

phantom. The Supporting Information is available free of charge on the ACS Publications website at DOI: 10.1021/acsami.5b02077.

AUTHOR INFORMATION

Corresponding Authors

*Y.Z. Tel: 023-63693709. E-mail: zhengyuanyi@gmail.com.
*Z.M. E-mail: meizhechuan@21cn.com.

Notes

The authors declare no competing financial interest.

ACKNOWLEDGMENTS

The authors thank Dr. Yuanqing Yao and Ling Jiang for their help in this study. We acknowledge financial support from the National Science Fund for Distinguished Young Scholars (no. 81425014), the 973 program (no. 2014CB744500), the National Nature Science Fund of China (nos. 81270021 and 8271598), the Chongqing Science Fund for Distinguished Young Scholars (no. cstc2013jcyjjq10004), the Program for New Century Excellent Talents in University of Ministry of Education of China (no. NCET-13-1067), the Key Grant of Education Commission of Chongqing (no. KJ120328), and the Key Grant of Chinese Ministry of Education (no. 212142).

REFERENCES

(1) Odle, T. G. Adverse Effects of Breast Cancer Treatment. *Radiologic Technol.* **2014**, *85*, 297M−319M (quiz 320M−323M)..

(2) Al-Ghazal, S. K.; Fallowfield, L.; Blamey, R. W. Comparison of Psychological Aspects and Patient Satisfaction Following Breast Conserving Surgery, Simple Mastectomy and Breast Reconstruction. *Eur. J. Cancer* **2000**, *36*, 1938−1943.

(3) Nguyen, T.; Hattery, E.; Khatri, V. P. Radiofrequency Ablation and Breast Cancer: A Review. *Gland Surg.* **2014**, *3*, 128−135.

(4) van Esser, S.; van den Bosch, M. A.; van Diest, P. J.; Mali, W. T.; Borel Rinkes, I. H.; van Hillegersberg, R. Minimally Invasive Ablative Therapies for Invasive Breast Carcinomas: An Overview of Current Literature. *World J. Surg.* **2007**, *31*, 2284−2292.

(5) Zhao, Z.; Wu, F. Minimally-Invasive Thermal Ablation of Early-Stage Breast Cancer: A Systemic Review. *Eur. J. Surg. Onco.* **2010**, *36*, 1149−1155.

(6) Zhao, L.; Yang, B.; Wang, Y.; Yao, Z.; Wang, X.; Feng, S. S.; Tang, J. Thermochemotherapy Mediated by Novel Solar-Planet Structured Magnetic Nanocomposites for Glioma Treatment. *J. Nanosci. Nanotechnol.* **2012**, *12*, 1024−1031.

(7) Schildkopf, P.; Ott, O. J.; Frey, B.; Wadepohl, M.; Sauer, R.; Fietkau, R.; Gaipl, U. S. Biological Rationales and Clinical Applications of Temperature Controlled Hyperthermia—Implications for Multimodal Cancer Treatments. *Curr. Med. Chem.* **2010**, *17*, 3045−3057.

(8) Jordan, A.; Scholz, R.; Wust, P.; Fahling, H.; Krause, J.; Wlodarczyk, W.; Sander, B.; Vogl, T.; Felix, R. Effects of Magnetic Fluid Hyperthermia (MFH) on C3h Mammary Carcinoma in Vivo. *Int. J. Hyperthermia* **1997**, *13*, 587−605.

(9) Rehman, J.; Landman, J.; Tucker, R. D.; Bostwick, D. G.; Sundaram, C. P.; Clayman, R. V. Ferromagnetic Self-Regulating Reheatable Thermal Rod Implants for in Situ Tissue Ablation. *J. Endourol.* **2002**, *16*, 523−531.

(10) Laurent, S.; Dutz, S.; Hafeli, U. O.; Mahmoudi, M. Magnetic Fluid Hyperthermia: Focus on Superparamagnetic Iron Oxide Nanoparticles. *Adv. Colloid Interface Sci.* **2011**, *166*, 8−23.

(11) El-Sayed, A. H.; Aly, A. A.; El-Sayed, N. I.; Mekawy, M. M.; El-Gendy, A. A. Calculation of Heating Power Generated from Ferromagnetic Thermal Seed (PdCo-PdNi-CuNi) Alloys Used as Interstitial Hyperthermia Implants. *J. Mater. Sci.: Mater. Med.* **2007**, *18*, 523−528.

(12) Latorre, M.; Rinaldi, C. Applications of Magnetic Nanoparticles in Medicine: Magnetic Fluid Hyperthermia. *P. R. Health Sci. J.* **2009**, *28*, 227−238.

(13) Chen, Y.; Jiang, L.; Wang, R.; Lu, M.; Zhang, Q.; Zhou, Y.; Wang, Z.; Lu, G.; Liang, P.; Ran, H.; Chen, H.; Zheng, Y. Injectable Smart Phase-Transformation Implants for Highly Efficient in Vivo Magnetic-Hyperthermia Regression of Tumors. *Adv. Mater.* **2014**, *26*, 7468−7473.

(14) Saillenfait, A. M.; Gallissot, F.; Sabate, J. P. Developmental Toxic Effects of *N*-Ethyl-2-pyrrolidone Administered Orally to Rats. *J. Appl. Toxicol.* **2007**, *27*, 491−497.

(15) Sitarek, K.; Stetkiewicz, J.; Wasowicz, W. Evaluation of Reproductive Disorders in Female Rats Exposed to *N*-Methyl-2-pyrrolidone. *Birth Defects Res., Part B* **2012**, *95*, 195−201.

(16) Takagi, S.; Chow, L. C.; Ishikawa, K. Formation of Hydroxyapatite in New Calcium Phosphate Cements. *Biomaterials* **1998**, *19*, 1593−1599.

(17) Burguera, E. F.; Xu, H. H.; Weir, M. D. Injectable and Rapid-Setting Calcium Phosphate Bone Cement with Dicalcium Phosphate Dihydrate. *J. Biomed. Mater. Res., Part B* **2006**, *77*, 126−134.

(18) Zhang, M.; Li, X. H.; Gong, Y. D.; Zhao, N. M.; Zhang, X. F. Properties and Biocompatibility of Chitosan Films Modified by Blending with PEG. *Biomaterials* **2002**, *23*, 2641−2648.

(19) Yuan, G.; Yuan, Y.; Xu, K.; Luo, Q. Biocompatible PEGylated Fe_3O_4 Nanoparticles as Photothermal Agents for Near-Infrared Light Modulated Cancer Therapy. *Int. J. Mol. Sci.* **2014**, *15*, 18776−18788.

(20) Han, B.; Ma, P. W.; Zhang, L. L.; Yin, Y. J.; Yao, K. D.; Zhang, F. J.; Zhang, Y. D.; Li, X. L.; Nie, W. β-TCP/MCPM-Based Premixed Calcium Phosphate Cements. *Acta Biomater.* **2009**, *5*, 3165−3177.

(21) Ventura, M.; Sun, Y.; Cremers, S.; Borm, P.; Birgani, Z. T.; Habibovic, P.; Heerschap, A.; van der Kraan, P. M.; Jansen, J. A.; Walboomers, X. F. A Theranostic Agent to Enhance Osteogenic and Magnetic Resonance Imaging Properties of Calcium Phosphate Cements. *Biomaterials* **2014**, *35*, 2227−2233.

(22) Burguera, E. F.; Xu, H. H.; Sun, L. Injectable Calcium Phosphate Cement: Effects of Powder-to-Liquid Ratio and Needle Size. *J. Biomed. Mater. Res., Part B* **2008**, *84*, 493−502.

(23) Kawashita, M.; Kawamura, K.; Li, Z. PMMA-Based Bone Cements Containing Magnetite Particles for the Hyperthermia of Cancer. *Acta Biomater.* **2010**, *6*, 3187−3192.

(24) Hilger, I.; Andra, W.; Bahring, R.; Daum, A.; Hergt, R.; Kaiser, W. A. Evaluation of Temperature Increase with Different Amounts of Magnetite in Liver Tissue Samples. *Invest. Radiol.* **1997**, *32*, 705−712.

(25) Kusaka, M.; Takegami, K.; Sudo, A.; Yamazaki, T.; Kawamura, J.; Uchida, A. Effect of Hyperthermia by Magnetite Cement on Tumor-Induced Bone Destruction. *J. Orthop. Sci.* **2002**, *7*, 354−357.

(26) Ge, F. T.; Zhao, S.; Niu, F.; Zhang, X. Treatment of Osteoporotic Vertebral Fractures with Percutaneous Balloon Kyphoplasty Using Calcium Phosphate Cement. *Zhongguo Gushang* **2014**, *27*, 128−132.

(27) Tanzawa, Y.; Tsuchiya, H.; Shirai, T.; Nishida, H.; Hayashi, K.; Takeuchi, A.; Kawahara, M.; Tomita, K. Potentiation of the Antitumor Effect of Calcium Phosphate Cement Containing Anticancer Drug and Caffeine on Rat Osteosarcoma. *J. Orthop. Sci.* **2011**, *16*, 77−84.

(28) Joosten, U.; Joist, A.; Frebel, T.; Brandt, B.; Diederichs, S.; von Eiff, C. Evaluation of an in Situ Setting Injectable Calcium Phosphate as a New Carrier Material for Gentamicin in the Treatment of Chronic Osteomyelitis: Studies in Vitro and in Vivo. *Biomaterials* **2004**, *25*, 4287−4295.

(29) Mohamed, M.; Borchard, G.; Jordan, O. In Situ Forming Implants for Local Chemotherapy and Hyperthermia of Bone Tumors. *J. Drug Delivery Sci. Technol.* **2012**, *22*, 393−408.

(30) Klammert, U.; Ignatius, A.; Wolfram, U.; Reuther, T.; Gbureck, U. In Vivo Degradation of Low Temperature Calcium and Magnesium Phosphate Ceramics in a Heterotopic Model. *Acta Biomater.* **2011**, *7*, 3469−3475.

(31) Ooms, E. M.; Egglezos, E. A.; Wolke, J. G.; Jansen, J. A. Soft-Tissue Response to Injectable Calcium Phosphate Cements. *Biomaterials* **2003**, *24*, 749−757.

DOI: 10.1021/acsami.5b02077
ACS Appl. Mater. Interfaces 2015, 7, 13866−13875

(32) Lu, J.; Descamps, M.; Dejou, J.; Koubi, G.; Hardouin, P.; Lemaitre, J.; Proust, J. P. The Biodegradation Mechanism of Calcium Phosphate Biomaterials in Bone. *J. Biomed. Mater. Res.* **2002**, *63*, 408−412.
(33) Mahmoudi, M.; Hofmann, H.; Rothen-Rutishauser, B.; Petri-Fink, A. Assessing the in Vitro and in Vivo Toxicity of Superparamagnetic Iron Oxide Nanoparticles. *Chem. Rev. (Washington, DC, U. S. A.)* **2012**, *112*, 2323−2338.
(34) Bourrinet, P.; Bengele, H. H.; Bonnemain, B.; Dencausse, A.; Idee, J.-M.; Jacobs, P. M.; Lewis, J. M. Preclinical Safety and Pharmacokinetic Profile of Ferumoxtran-10, an Ultrasmall Superparamagnetic Iron Oxide Magnetic Resonance Contrast Agent. *Invest. Radiol.* **2006**, *41*, 313−324.
(35) Minami, Y.; Kudo, M. Radiofrequency Ablation of Hepatocellular Carcinoma: A Literature Review. *Int. J. Hepatol.* **2011**, DOI: 10.4061/2011/104685.
(36) Cavallo Marincola, B.; Pediconi, F.; Anzidei, M.; Miglio, E.; Di Mare, L.; Telesca, M.; Mancini, M.; D'Amati, G.; Monti, M.; Catalano, C.; Napoli, A. High-Intensity Focused Ultrasound in Breast Pathology: Non-Invasive Treatment of Benign and Malignant Lesions. *Expert Rev. Med. Devices* **2015**, *12*, 191−199.
(37) Kim, Y. S. Advances in MR Image-Guided High-Intensity Focused Ultrasound Therapy. *Int. J. Hyperthermia* **2015**, *31*, 225−232.

DOI: 10.1021/acsami.5b02077
ACS Appl. Mater. Interfaces 2015, 7, 13866−13875